

Green's Function Monte Carlo for Lattice Fermions: Application to the t-J model

E. Manousakis
Florida State University, Tallahassee, FL 32306-3016

January 12, 2012

Outline

- 1 Trial state optimization
- 2 $O(N)$ Calculation of superexchange
- 3 Phase Separation
- 4 Spin and Charge Structure Factors
- 5 Phase Diagram of the $t - J$ Model
- 6 Comparison with other calculations
- 7 Conclusions

- 1 Trial state optimization
- 2 $O(N)$ Calculation of superexchange
- 3 Phase Separation
- 4 Spin and Charge Structure Factors
- 5 Phase Diagram of the $t - J$ Model
- 6 Comparison with other calculations
- 7 Conclusions

Trial state optimization

It is important that we start the GFMC with good trial and guiding states. In this section, we describe our method for optimizing these functions.

In continuum systems, one usually assumes a functional form for the trial and guiding functions and optimizes a function of the energy to find the best variational parameters. On a lattice, there are only a finite number of distances \mathbf{r} or equivalently wave vectors \mathbf{k} in any given simulation, so we allow the functions in the trial and guiding functions to have a parameter describing each distance or wave vector not related by symmetry.

For the Jastrow pair factors, $f(\mathbf{r})$ and $g(\mathbf{r})$, we apply all rotational and mirror symmetries. Translational symmetry is always assumed. However, we insist only on the mirror symmetries about the axes for the Fermion pairing field $a_{\mathbf{k}}$, so the function may be any linear combination of an s and $d_{x^2-y^2}$ pairing state. The mirror symmetry excludes d_{xy} symmetry.

Trial state optimization (Continued)

For a 20×20 lattice, we have 172 parameters for the trial state and 192 parameters for the guiding function with the pairing term. We tried optimizing several functions of the energy, but found minimizing the variance of the local energy to be the most robust [Umrigar et al., 1988]. We generate a set of configurations $\{\alpha_1, \alpha_2, \dots, \alpha_m\}$ distributed according to a weight w_{α_i} . The configurations remain the same throughout the minimization procedure. We minimize the function

$$\sigma^2 = \frac{\sum_{i=1}^m [H\Psi_{\alpha_i}^T/\Psi_{\alpha_i}^T - E]^2 |\Psi_{\alpha_i}^T|^2 / w_{\alpha_i}}{\sum_{i=1}^m |\Psi_{\alpha_i}^T|^2 / w_{\alpha_i}}, \quad (1)$$

where E is a guess for the ground state energy that we determine self consistently. We use the same function to optimize both our trial and guiding functions.

Trial state optimization (Continued)

With a finite random walk, the calculation of the energy in (1) uses many more states than the calculation of the norm.

Occasionally, this created instabilities, which we cured by deriving another way of calculating the norm using all the neighbors in the random walk. We may write

$$\langle \Psi | \Psi \rangle = \sum_{\alpha} |\Psi_{\alpha}|^2 \quad (2)$$

$$= \sum_{\alpha} \left(|\Psi_{\alpha}|^2 (1 - A_{\alpha}) + B_{\alpha} \sum_{\beta \in \{H_{\alpha}\}} |\Psi_{\beta}|^2 \right) \quad (3)$$

where $\{H_{\alpha}\}$ is the set of all states neighboring $|\alpha\rangle$ by application of the Hamiltonian. We see (3) follows from (2) if we choose $B_{\alpha} = C$ and $A_{\alpha} = CN_{\alpha}$ for some constant C , where N_{α} is the number of neighbors of $|\alpha\rangle$ where Ψ does not vanish. Since this version of the norm is calculated from all the states entering the energy, no factors in the numerator of (1) are absent from the

Trial state optimization (Continued)

We calculate the effective number of configurations contributing to the normalization as

$$N_{\text{eff}} = \left(\sum_{i=1}^m \frac{|\Psi_{\alpha_i}^T|^2}{w_{\alpha_i}} \right)^2 / \sum_{i=1}^m \frac{|\Psi_{\alpha_i}^T|^4}{w_{\alpha_i}^2}. \quad (4)$$

This quantity approaches n if all states contribute equally and drops to 1 as one state begins to dominate [Alexander et al., 1992]. We adjust the length of our random walks so N_{eff} is at least 10 times the number of parameters being optimized.

Close to phase separation, the standard Metropolis algorithm develops a small acceptance ratio, and tends to stay in the same configuration for many steps. In order to sample phase space quickly, we choose our configurations using a transition probability in which H is the off-diagonal part of the Hamiltonian, ensuring a new configuration with each move. Thus the configurations are distributed according to the weight $w_{\alpha_i} = z_{\alpha_i} |\Psi_{\alpha_i}^G|^2$.

- 1 Trial state optimization
- 2 $O(N)$ Calculation of superexchange**
- 3 Phase Separation
- 4 Spin and Charge Structure Factors
- 5 Phase Diagram of the $t - J$ Model
- 6 Comparison with other calculations
- 7 Conclusions

$O(N)$ Calculation of superexchange

In the GFMC projection, we need to calculate the local energy $E_{\alpha_i} = \sum_{\beta} \langle \Psi_{\beta} | H | \Psi_{\alpha_i} \rangle$ for the guiding wave function, Ψ^G , at each step of the random walk. Due to the simplicity of (??), the local energy can be calculated efficiently in $O(N)$ steps. Only the amplitude of the trial state Ψ^T is needed at each step.

In section 4, we describe the procedure used to optimize the trial function we use in the GFMC. The method is most efficient when the local energy if the function can be calculated quickly. For a determinantal function, the local kinetic energy takes $O(N)$ per particle, so it scales as $O(N^2)$ for the system. The superexchange term in the t - J model, $\sum_{\langle ij \rangle} S_i^+ S_j^-$, exchanges two particles, changing both a row and a column of the determinant (??). In this section, we show how the amplitude of swapping two particles may be calculated in $O(N)$ steps.

$O(N)$ Calculation of superexchange (Continued)

Suppose we swap the m 'th up electron with the n 'th down electron. We will modify both row m and column n in the determinant. We write the new elements as $D_{mj} \rightarrow r_j$ and $D_{in} \rightarrow c_i$. Naturally, $r_n = c_m$. One can show the ratio of the determinant before and after the swap is

$$\frac{|\mathbf{D}'|}{|\mathbf{D}|} = \left(\sum_i r_i I_{im} \right) \left(\sum_j I_{nj} c_j \right) + I_{nm} c_m - I_{nm} \sum_{ij} r_i I_{ij} c_j. \quad (5)$$

Direct evaluation of the sum $S = \sum_{ij} r_i I_{ij} c_j$ takes $O(N^2)$ per pair of neighboring particles. For this reason, many researchers evaluate the superexchange term only every N Monte Carlo steps [Gros, 1989].


Our trick is to evaluate S once when a pair of particles become nearest neighbors, and then to update it in $O(N)$ steps for any

$O(N)$ Calculation of superexchange (Continued)

Suppose the l 'th up electron moves ($l \neq m$), altering row l in the determinant (??), so $D_{lj} \rightarrow s_j$. The inverse I is updated according to (??) and $c_l \rightarrow c'_l$ takes a new value.

We can write the new sum S' in terms of the old sum and extra factors as

$$\begin{aligned}
 S' &= \sum_{ij} r_i I'_{ij} c'_j \\
 &= \sum_{ij} r_i \left(I_{ij} \left(1 + \frac{1}{\gamma_l} \delta_{lj} \right) - \frac{1}{\gamma_l} I_{il} \sum_k s_k I_{kj} \right) c'_j \quad (6) \\
 &= S + \frac{1}{\gamma_l} \left(\sum_i r_i I_{il} \right) \left(c'_l - \sum_j \gamma_j c_j \right)
 \end{aligned}$$

where $\gamma_j = \sum_k s_k I_{kj}$ is used in the inverse update. This calculation requires only $O(N)$ steps, so the local superexchange energy of the system may be evaluated in $O(N^2)$ time. 

- 1 Trial state optimization
- 2 $O(N)$ Calculation of superexchange
- 3 Phase Separation**
 - Maxwell Construction
 - Approach
 - Results at $J = t$
 - Results in the $J < t$ Region
 - Results near J_c^B
 - Results below J_c^B
- 4 Spin and Charge Structure Factors
- 5 Phase Diagram of the $t - J$ Model
- 6 Comparison with other calculations
- 7 Conclusions

Maxwell Construction

In the 1D tJ model phase separation has been determined using

- Divergence of the density structure factor at long wavelengths.
- Divergence of the compressibility as determined from the second derivative of the energy with respect to electron or hole density.

In the 1D model, phase separation occurs between two regions,

- one with no electrons
- and one containing some electrons and some holes.

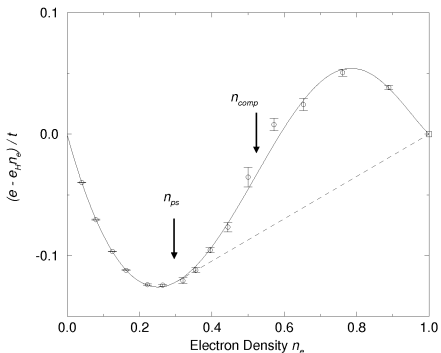
For a finite system, electrons may tunnel through the vacuum, lowering the ground state energy. For this reason, the inverse compressibility actually passes through zero and becomes slightly negative. This effect is a surface effect and vanishes in the limit of infinite system size.

Maxwell Construction(cont'd)

- In the 2D t - J model, the Fermi surface can change dramatically with electron density for a given system size. These shell effects make accurate comparisons of energies calculated with different numbers of electrons impossible.
- Other studies used a vanishing inverse compressibility as the criterion for the onset of phase separation [Putikka et al., 1992b, Putikka et al., 1992a, Poilblanc, 1995, Jarrell and Gubernatis, 1995]. The compressibility is not the proper observable to find the phase-separation boundary in the 2D t - J model, where the transition is first order.
- The compressibility diverges in the phase separation region, but it jumps at the boundary with the uniform phase.
- This discontinuity is difficult to see due to the surface energy of the two coexisting phases. In the region of phase separation, the compressibility suffers strong finite-size effects due to large surface energy of the two coexisting phases.

Maxwell Construction (cont'd)

The ground-state energy per site at $J = 2.5t$ for 32 electrons. For clarity, the energies are shifted by a linear factor, $-e_H n_e$. The circles with error bars show the energies calculated on lattices of dimensions 6×6 , 7×7 , ..., 28×28 . Solid line: A sixth-order polynomial fit to the data.



At any electron density in the range, $n_{ps} < n_e < 1$, the system can reduce its energy by separating into two regions with densities $n_A = n_{ps}$ and $n_B = 1$, resulting in an energy given by the dashed line at the average density. Onset of phase separation occurs at $n_{ps} = 0.296 \pm 0.004$ while the inverse compressibility vanishes at $n_{comp} = 0.52 \pm 0.10$.

Maxwell Construction (cont'd)

Maxwell Construction (cont'd)

- The ground state of the infinite system at $n_e > n_{ps}$ cannot be a uniform phase, because the energy of the uniform phase, $e(n_e)$, is higher than $e_{ps}(n_e)$ at the same density. The dashed straight line, $e_{ps}(n_e)$, is the energy of a mixture of two phases, one at electron density $n_A = 1$ and the other at electron density $n_B = n_{ps}$. The infinite system phase separates into these two regions. (Maxwell construction).

Maxwell Construction (cont'd)

- The ground state of the infinite system at $n_e > n_{ps}$ cannot be a uniform phase, because the energy of the uniform phase, $e(n_e)$, is higher than $e_{ps}(n_e)$ at the same density. The dashed straight line, $e_{ps}(n_e)$, is the energy of a mixture of two phases, one at electron density $n_A = 1$ and the other at electron density $n_B = n_{ps}$. The infinite system phase separates into these two regions. (Maxwell construction).
- In order to be stable, the energy of the infinite system must be concave everywhere. Given the solid line and the allowed density range of the t-J model, the dashed line drawn in the figure is the only line possible to make the energy of the infinite system globally convex. This energy is given by the solid line for $n_e < n_{ps}$ and the dashed line for $n_e > n_{ps}$.

Maxwell Construction (cont'd)

Maxwell Construction (cont'd)

- The density of one of the constituent phases, the Heisenberg phase at $n_e = 1$, lies at an extreme limit of the allowed density range. It is not possible to add electrons to the Heisenberg solid beyond $n_e = 1$ so the dashed line is tangent to the fitting curve at $n_e = n_{ps}$ and not at $n_e = 1$. If the t-J model did allow $n_e > 1$, the intersection point of the solid and dashed lines would be shifted to higher densities.

Maxwell Construction (cont'd)

- The density of one of the constituent phases, the Heisenberg phase at $n_e = 1$, lies at an extreme limit of the allowed density range. It is not possible to add electrons to the Heisenberg solid beyond $n_e = 1$ so the dashed line is tangent to the fitting curve at $n_e = n_{ps}$ and not at $n_e = 1$. If the t-J model did allow $n_e > 1$, the intersection point of the solid and dashed lines would be shifted to higher densities.
- We never examined systems with densities $n_e \gtrsim 0.94$, so we cannot exclude the re-entrance of a homogeneous phase in this region. For such a phase to be stabilized, the solid curve would have to drop back below the dashed line in this density range. We never saw any indication of this possibility at any J/t . If a re-entrant homogeneous phase did exist, the new Maxwell line would lie slightly below the one drawn and would be tangent to the solid curve at both intersections, but the phase-separated region would persist at densities $n_e \lesssim 0.94$.

Approach

- We use Maxwell construction to determine the phase separation boundary.
- We minimize the shell-effects when varying the electron-density by keeping the number of electrons fixed at a closed shell configuration and changing the size of the lattice.
- We choose our number of electrons so that they always correspond to closed shell configuration. This choice eliminates possible degeneracies of states at the Fermi level. Such degeneracies might favor flatness of the energy as a function of density which might be mistaken for phase separation.
- An additional (technical reason) for wanting to keep closed shell configurations is that on a finite lattice it leads to an energy gap between the ground state and the first excited state which helps our projection method to converge.

Results at $J = t$

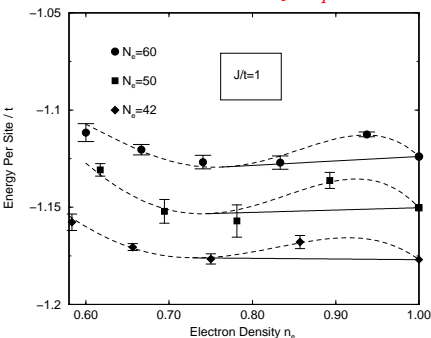
Size dependence of the critical value of electron density n_{ps} for phase separation.

Bottom: $N_e = 42$ and $N_s = 49, 56, 64, 72, 81, 90$.

Middle: $N_e = 50$ and $N_s = 56, 64, 72, 81, 90$.

Top: $N_e = 60$ and $N_s = 64, 72, 81, 90, 100, 110, 121$.

Each curve has been shifted by 0.025.



The value of n_{ps} is determined by a cubic polynomial fit and using the corresponding energy for the lattice full of electrons calculated for the same number of electrons. This can be done using the GFMC results for the undoped system and the extrapolation

$$E/N = e_0 + \lambda N^{-3/2} \quad (7)$$

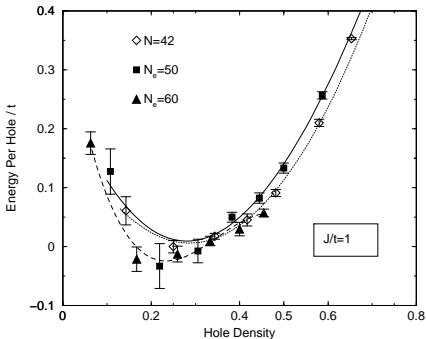
Results at $J = t$ (Cont'd)

Individually, each number of electrons is consistent with a solution where a line beginning from the no-hole limit ($n_e = 1$) and being tangent on the polynomial (that fits the data points) near $n_e = 0.745$. Therefore we conclude that the finite-size effects are small in our method of determining n_{ps} and the phase separation density for $J/t = 1$ is $n_{ps} = 0.745 \pm 0.015$.

Results at $J = t$ (Cont'd)

Using the energy per hole. Shell effects

The energy per hole at $J = t$ for $N_e = 42$ (open diamonds) $N_e = 50$ (solid squares) and $N_e = 60$ (solid circles). The minimum is at about the same value as that determined by the tangent construction.



Notice, however, this method of using all the size lattices together suffers from shell effects which have a non-monotonic effect with size. That is why it is essential to compare systems with the same number of electrons. The shell effects are systematic errors that affect the other calculations which have been recently appeared in the literature which we discuss in this paper.

Results in the $J < t$ Region

The ground-state energy per site at $J = 0.5t$

Top: $N_e = 32$ and

$N_s = 36, 49, 56, 64, 72, 81, 90$

Second: $N_e = 42$ and

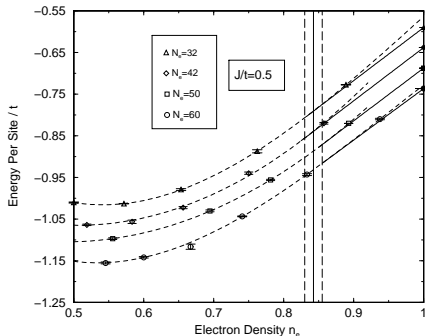
$N_s = 49, 56, 64, 72, 81, 90$

Third: $N_e = 50$ and

$N_s = 56, 64, 72, 81, 90$

Bottom: $N_e = 60$ and $N_s =$

$49, 56, 64, 72, 81, 90, 100, 110$



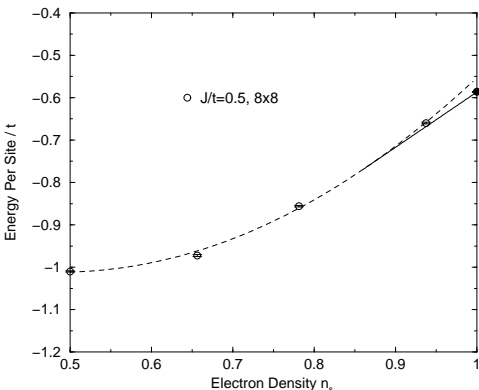
Individually, each number of electrons is consistent with a value of n_{ps} near $n_e = 0.84$. Clearly the 42 electron data doesn't prove that there is a clear tangent at this value of n_e , but the data is consistent with this value. Therefore we conclude that the finite-size effects are small in our method of determining n_{ps} and the phase separation density for $J/t = 0.5$ is $n_{ps} = 0.843 \pm 0.015$.

Results in the $J < t$ Region

Demonstration of the significance of shell effects

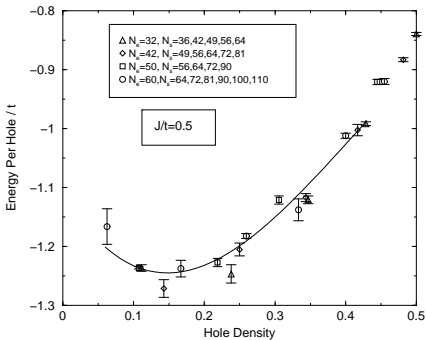
The energy per site at $J = 0.5t$ for an 8×8 lattice for 32, 42, 50 and 60 electrons. To demonstrate the role of shell effects, here we keep the lattice size fixed and we vary n_e . Notice that even-though these data also give the same phase separation density within error bars as that determined by

our method described before, the shell effects are large. Such deviations from a smooth curve could lead us to drawing the wrong conclusions about phase separation boundaries.



Results in the $J < t$ Region

Energy per hole. The energy per hole at $J = 0.5t$ for 32, 42, 50 and 60 electrons.



The curve attains a minimum at approximately the same value as that determined by the tangent construction at the cubic polynomial fit of the energy per size for a given number of electrons. Notice, again, the shell effects.

Results near J_c^B

Using GFMC Boninsegni and Manousakis [Boninsegni and Manousakis, 1993](BM) studied the motion of one and two holes using transient estimate.

- They found that two holes form a d-wave bound state.
- They found a critical value $J_c^B \simeq 0.27t$ of J/t below which there is no two-hole d-wave bound state. This value of J_c^B was determined by calculating the binding energy for two holes on lattices up to 8×8 . BM noticed that because the bound state wave function decays exponentially with distance the finite size effects were rather small.
- They pursued a finite-size analysis from which they determined J_c^B .

Thus, we choose the $J/t = 0.3$ to examine the question of phase separation believing that this value is very close to the critical value J_c^B .

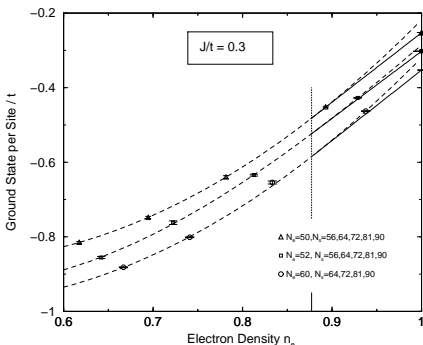
Results near J_c^B Phase separation for $J/t = 0.3$

The ground-state energy per site at $J = 0.3t$ for 50, 52 and 60 electrons and lattices of sizes

$N_s = 56, 64, 72, 81, 90,$

$N_s = 56, 64, 72, 81, 90$ and

$N_s = 64, 72, 81, 90$ respectively.



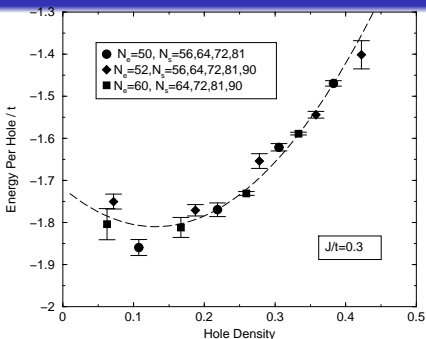
Notice that the values of J_c/t determined from these sets of data are very close. We obtain: $n_e = 0.877 \pm 0.010$.

Results near J_c^B

Energy per hole

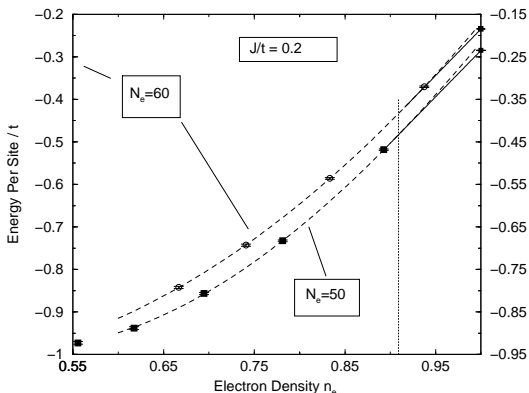
The energy per hole at $J = 0.3t$ for 50, 52 and 60 electrons.

There is a minimum at $n_{ps} = 0.12$ which agrees very well with the value obtained from the tangent construction.



The single-hole energy can be estimated by fitting the calculated values for that as a function of J/t to a form $E = E_0 + aJ^{2/3}$. The two-hole binding energy for $J/t = 0.3$ can be estimated using the formula which were used by Boninsegni and Manousakis to obtain the critical value of J_c^B . Thus, we can obtain a value for the energy per hole, assuming that holes are bound in pairs and they form a dilute gas of hole-pairs. This value of this energy is higher than the value of the energy per hole at the minimum of our curve.

Results below J_c^B

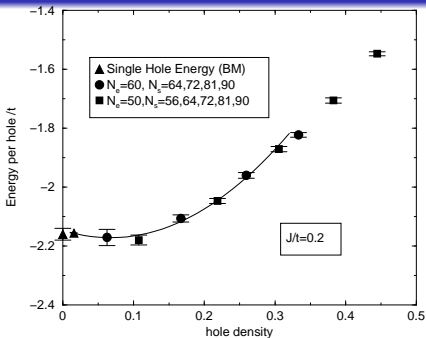


The ground-state energy per site at $J = 0.2t$ for 50 and 60 electrons and lattices with sizes $N_s = 56, 64, 72, 81, 90$ and $N_s = 64, 72, 81, 90$ respectively. Notice again that the values of J_c/t determined from the two sets of data are very close, we find: $n_{ps} = 0.909 \pm 0.008$.

Results below J_c^B

The energy per hole at $J = 0.2t$ for 50 and 60 electrons. The **single-hole energy** as obtained from Boninsegni and Manousakis [Boninsegni and Manousakis, 1992, Boninsegni and Manousakis, 1993] is also plotted for 8×8 and 10×10 size lattices.

Below J_c^B where there is no two-hole d-wave bound state, if there is no phase separation the minimum energy per hole should be the single-hole energy at zero hole density. At $J/t = 0.2$ the single-hole energy was also calculated by Boninsegni and Manousakis for an 8×8 and 10×10 size lattices. This value of the energy is shown and it is clearly higher than the minimum of the energy per hole curve which occurs at approximately hole density of $x = 0.09$.



- 1 Trial state optimization
- 2 $O(N)$ Calculation of superexchange
- 3 Phase Separation
- 4 Spin and Charge Structure Factors**
- 5 Phase Diagram of the $t - J$ Model
- 6 Comparison with other calculations
- 7 Conclusions

Spin and Charge Structure Factors

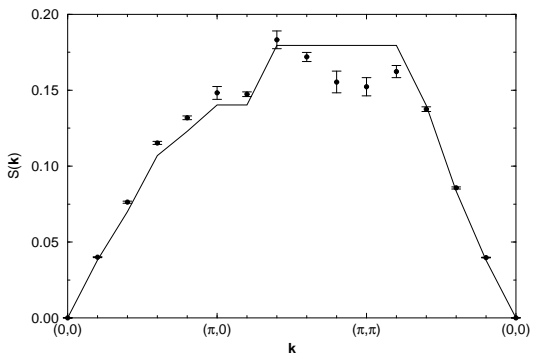


Figure: Our calculated spin-structure factor as a function of \vec{k} is compared with that obtained with the Gutzwiller wavefunction (solid line).

Spin and Charge Structure Factors

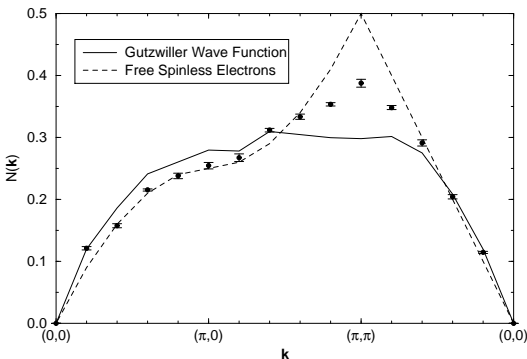
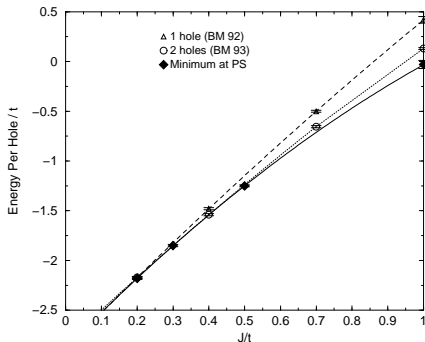


Figure: Our calculated density-structure factor as a function of \vec{k} is compared with that obtained with the Gutzwiller wavefunction (solid line).

- 1 Trial state optimization
- 2 $O(N)$ Calculation of superexchange
- 3 Phase Separation
- 4 Spin and Charge Structure Factors
- 5 Phase Diagram of the $t - J$ Model**
- 6 Comparison with other calculations
- 7 Conclusions

Phase Diagram of the $t - J$ Model

The energy per hole at the density where the phase separation minimum occurs as a function of J/t (solid line). This is compared to the energy per hole obtained from the single hole calculation of Boninsegni and Manousakis ('92) (dashed line) and to the energy per hole obtained from the 2 hole calculation of Boninsegni and Manousakis ('93).



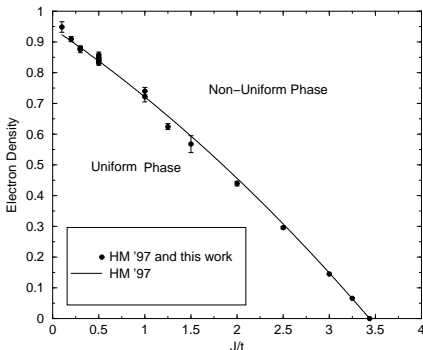
Notice that while the dashed line and the dotted line meet at $J/t \sim 0.3$, the minimum at the phase separation density and the dotted line do not meet. Notice that the additional energy gained to to phase separation decreases with decreasing J/t as expected.

Phase Diagram of the $t - J$ Model

The phase separation boundary.

The phase diagram as calculated using the present method and the Maxwell construction. A more complete phase diagram for the 2D $t - J$ model as a function of J/t and doping was given in Fig. 3 of Ref.

[Hellberg and Manousakis, 1997].

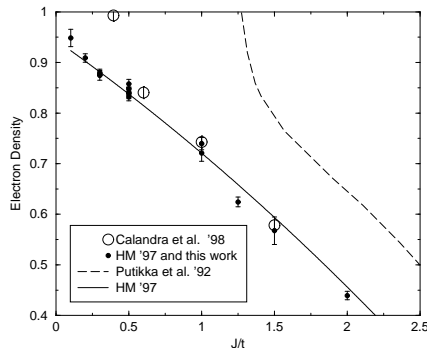


That phase diagram is also accurate in the low density region where exact (in the zero density limit) or controllable calculations can be done.

- 1 Trial state optimization
- 2 $O(N)$ Calculation of superexchange
- 3 Phase Separation
- 4 Spin and Charge Structure Factors
- 5 Phase Diagram of the $t - J$ Model
- 6 Comparison with other calculations**
- 7 Conclusions

Comparison with other calculations

Comparison of our results with those obtained by Putikka et al. [Putikka et al., 1992b] (High Temperature Series expansion) and by Callandra Becca and Sorella (CBS) [Callandra M. and Sorella, 1998] (circles).



Notice that our phase diagram and that of CBS are very close except in the delicate physical region of small J/t .

Comparison with other calculations (Cont'd)

Therefore, we can draw a relatively strong conclusion from this comparison:

Main conclusion

The conclusion drawn from the early studies of the $t - J$ model [Putikka et al., 1992b, Dagotto, 1994] that the physical region of the model is safely away from the phase separation boundary is not correct.

What our work and the work of CBS find is that the interesting region of J/t is either next to the phase separation boundary or inside the phase separated region. In both cases phase separation fluctuations could play an important role in the mechanism for superconductivity in the copper oxides.

Comparison with other calculations

There is also an important difference between our results and those of CBS.

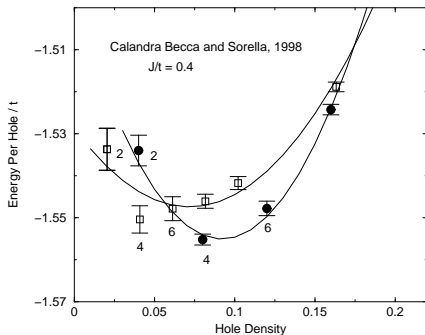
Main Difference

Our results indicate that phase separation in the $t - J$ model is present for all J/t , while the conclusion of CBS is that there is a finite value of $J/t \simeq 0.4$ below which there is no phase separation. The reason for this disagreement is that this region requires a very high degree of accuracy in the numerical results.

We would like to discuss the results of CBS where they find that at $J/t = 0.4$ there is no phase separation for lattices of size $N_s = 98$.

Comparison with other calculations

Fits of the results obtained by CBS for 50 sites (solid circles) and 98 (open squares) to a quadratic polynomial. The result for the lowest value of x for the 98 site system was not included in the original 98 publication by CBS, it was calculated by CBS after our request.



Without using the point which corresponds to the lowest value of x , CBS concluded that the fact that we found PS at $J/t = 0.4$ was a finite-size effect. Notice that after the inclusion of the most recently calculated point for the 98-site system there is still a minimum at somewhat lower value of $x_c = 0.072$. This value of x_c is close to our value for phase separation which is about 0.1 for $J/t = 0.4$.

Comparison with other calculations

Let us now examine more specifically the results in the previous Figure. We have labeled by 2,4,6 the points which correspond to 2,4,6 holes in the 50 and 98 site lattices. Notice that the energy of 4 holes is the same within error bars in both lattices. The same is true for the 6 hole case. Thus, the energy for 2,4 and 6 holes *seems* to be independent of the size of the lattice within error bars. This can be either a) a genuine characteristic of presence of phase separation where the two, four and six-hole bubbles in a much larger system do not feel the size effects because they are self bound at a characteristic size much smaller than the total system or b) a result of shell-effects which we have discussed and are minimized in our calculation or c) the calculation of CBS has larger systematic or statistical errors than those reflected by their error bars.

- 1 Trial state optimization
- 2 $O(N)$ Calculation of superexchange
- 3 Phase Separation
- 4 Spin and Charge Structure Factors
- 5 Phase Diagram of the $t - J$ Model
- 6 Comparison with other calculations
- 7 Conclusions**

Conclusions

Conclusions

- We have developed an efficient Quantum Monte Carlo method which resembles the GFMC method where without eliminating the minus-sign the fluctuations are controlled with the aid of appropriately constructed guiding functions up to a certain high power of the Green's function.

Conclusions

- We have developed an efficient Quantum Monte Carlo method which resembles the GFMC method where without eliminating the minus-sign the fluctuations are controlled with the aid of appropriately constructed guiding functions up to a certain high power of the Green's function.
- Starting from a good initial state allows us to achieve convergence before the statistical errors become too large.

Conclusions

- We have developed an efficient Quantum Monte Carlo method which resembles the GFMC method where without eliminating the minus-sign the fluctuations are controlled with the aid of appropriately constructed guiding functions up to a certain high power of the Green's function.
- Starting from a good initial state allows us to achieve convergence before the statistical errors become too large.
- We developed a powerful technique which uses **all** the calculated powers of the Hamiltonian to **extrapolate** to infinite power.

Conclusions

- We have developed an efficient Quantum Monte Carlo method which resembles the GFMC method where without eliminating the minus-sign the fluctuations are controlled with the aid of appropriately constructed guiding functions up to a certain high power of the Green's function.
- Starting from a good initial state allows us to achieve convergence before the statistical errors become too large.
- We developed a powerful technique which uses **all** the calculated powers of the Hamiltonian to **extrapolate** to infinite power.
- This technique comes also with solutions to a number of other technical problems such as:

Conclusions

- We have developed an efficient Quantum Monte Carlo method which resembles the GFMC method where without eliminating the minus-sign the fluctuations are controlled with the aid of appropriately constructed guiding functions up to a certain high power of the Green's function.
- Starting from a good initial state allows us to achieve convergence before the statistical errors become too large.
- We developed a powerful technique which uses **all** the calculated powers of the Hamiltonian to **extrapolate** to infinite power.
- This technique comes also with solutions to a number of other technical problems such as:
 - a) enabling the guided random walk to walk through the nodes with an $O(N^2)$ algorithm using the idea of **"detour walk"**. This does not restrict our calculation within the fixed node approximation.

Conclusions (Cont'd)

Conclusions (Cont'd)

- b) instead of using multiple walkers the introduction of a single walker whose walk is very long allows us to compute all the desired powers of H^m $m = 0, 1, \dots, p_{max}$ in parallel by looking back in the past p_{max} steps of the walk.

Conclusions (Cont'd)

- b) instead of using multiple walkers the introduction of a single walker whose walk is very long allows us to compute all the desired powers of H^m $m = 0, 1, \dots, p_{max}$ in parallel by looking back in the past p_{max} steps of the walk.
- This technique was applied to the two-dimensional $t - J$ model to investigate its phase diagram. It is found, contrary to most previous studies except the original work of Emery Kivelson and Lin, that there is phase separation (PS) at **all interaction strengths** of the $t - J$ model. The signal for phase separation is clear when one takes care of the following additional difficulties:

Conclusions (Cont'd)

- b) instead of using multiple walkers the introduction of a single walker whose walk is very long allows us to compute all the desired powers of H^m $m = 0, 1, \dots, p_{max}$ in parallel by looking back in the past p_{max} steps of the walk.
- This technique was applied to the two-dimensional $t - J$ model to investigate its phase diagram. It is found, contrary to most previous studies except the original work of Emery Kivelson and Lin, that there is phase separation (PS) at **all interaction strengths** of the $t - J$ model. The signal for phase separation is clear when one takes care of the following additional difficulties:
- First, Maxwell construction is the cleanest and strongest signal for PS because it suffers the least from finite-size effects.








Conclusions (Cont'd)






Conclusions (Cont'd)

- Second the **shell-effects can mask** the signal because the energy as a function of density when one keeps the size of the lattice constant and varies the density by varying the electron number is not a smooth curve. The reason for that is that the kinetic energy of the electrons changes by a finite amount when adding an electron to a new shell.

Conclusions (Cont'd)

- Second the **shell-effects can mask** the signal because the energy as a function of density when one keeps the size of the lattice constant and varies the density by varying the electron number is not a smooth curve. The reason for that is that the kinetic energy of the electrons changes by a finite amount when adding an electron to a new shell.
- We have chosen to keep the electron number fixed at a **closed shell** configuration and change the size of the lattice. The number of electrons which form closed shell configurations depends on the boundary conditions.

-  Alexander, S. A., Coldwell, R. L., and Morgan, J. D. (1992).
J. Chem. Phys., 97:8407.
-  Boninsegni, M. and Manousakis, E. (1992).
Phys. Rev. B, 46:560.
-  Boninsegni, M. and Manousakis, E. (1993).
Phys. Rev. B, 47:11897.
-  Calandra M., F. B. and Sorella, S. (1998).
Phys. Rev. Lett., 81:5185.
-  Dagotto, E. (1994).
Rev. Mod. Phys., 66:763.
-  Gros, C. (1989).
Ann. Phys. (NY), 189:53.
-  Hellberg, C. S. and Manousakis, E. (1997).
Gfmc for lattice fermions.
Phys. Rev. Lett., 78:4609.

-  Jarrell, M. and Gubernatis, J. E. (1995).
Phys. Rev. B, 00:0000.
-  Luchini, M. U., Ogata, M., Putikka, W. O., and Rice, T. M. (1991).
Phase diagram of the t-j model.
Physica C, 185-189:141.
-  Poilblanc, D. (1995).
Phase diagram of the two-dimensional t-j model at low doping.
Phys. Rev. B, 52:9201.
-  Putikka, W. O., Luchini, M. U., and Ogata, M. (1992a).
Ferromagnetism in the two-dimensional t-j model.
Phys. Rev. Lett., 69:2288.
-  Putikka, W. O., Luchini, M. U., and Rice, T. M. (1992b).
Aspects of the phase diagram of the two-dimensional t-j model.

Phys. Rev. Lett., 68:538.



Umrigar, C. J., Wilson, K. G., and Wilkins, J. W. (1988).

Phys. Rev. Lett., 60:1719.



White, S. and Scalapino, D. J. (1999).

Comparison.

preprint, xxx:xxx.